Crystals **2015**, *5*, 47-60; doi:10.3390/cryst5010047

OPEN ACCESS

crystals

ISSN 2073-4352

www.mdpi.com/journal/crystals

Article

High-Yield Synthesis of Helical Carbon Nanofibers Using Iron Oxide Fine Powder as a Catalyst

Yoshiyuki Suda [1,*], Koji Maruyama [1], Tetsuo Iida [1], Hirofumi Takikawa [1], Hitoshi Ue [2], Kazuki Shimizu [3] and Yoshito Umeda [4]

[1] Department of Electrical and Electronic Information Engineering, Toyohashi University of Technology, Toyohashi, Aichi 441-8580, Japan

[2] Fuji Research Laboratory, Tokai Carbon Co., Ltd., Oyama, Shizuoka 410-1431, Japan

[3] Development Department, Shonan Plastic Manufacturing Co., Ltd., Hiratsuka, Kanagawa 254-0807, Japan

[4] Corporate Research Department, Toho Gas Co., Ltd., Nagoya, Aichi 456-8511, Japan

***** Author to whom correspondence should be addressed; E-Mail: suda@ee.tut.ac.jp; Tel.: +81-532-44-6726; Fax: +81-532-44-6757.

Academic Editor: Daniele Gozzi

Received: 15 September 2014 / Accepted: 22 December 2014 / Published: 8 January 2015

Abstract: Carbon nanocoil (CNC), which is synthesized by a catalytic chemical vapor deposition (CCVD) method, has a coil diameter of 300–900 nm and a length of several tens of μm. Although it is very small, CNC is predicted to have a high mechanical strength and hence is expected to have a use in nanodevices such as electromagnetic wave absorbers and field emitters. For nanodevice applications, it is necessary to synthesize CNC in high yield and purity. In this study, we improved the conditions of catalytic layer formation and CCVD. Using optimized CVD conditions, a CNC layer with a thickness of >40 μm was grown from a $SnO_2/Fe_2O_3/SnO_2$ catalyst on a substrate, and its purity increased to 81% ± 2%.

Keywords: carbon nanocoil; carbon nanomaterials; chemical vapor deposition; nanodevices; catalyst metals

1. Introduction

Nanotechnology holds potential not only for miniaturization, densification, and increasing device performance but also for changing nanometer-scale physical properties and creating products with novel functions [1]. Therefore, materials for nanotechnology are now intensively researched. Among them, carbon nanomaterials have attracted considerable attention since the discovery of fullerene in 1985 [2]. Carbon nanotubes (CNTs) [3,4] and various types of carbon nanofibers (CNFs) [5] have also drawn increasing attraction.

In 1990, Motojima *et al.* [6] synthesized carbon microcoil (CMC), which is a regular-shaped helical carbon fiber, via catalytic chemical vapor deposition (CCVD) using a Ni catalyst-coated graphite substrate and feedstock gases (C_2H_2, H_2, N_2, and C_4H_4S). Motojima *et al.* [7] suggested that the growth mechanism of CMCs involved carbon segregation from the crystal facets of the catalyst nanoparticles.

After the discovery of CMC, the growth of carbon nanocoil (CNC), which is also a helical fiber and has a coil diameter of several hundreds of nanometers, was reported [8]. CNCs can be grown using Fe-coated indium-tin-oxide (ITO) and Ni-coated Cu substrates [8–10]. Furthermore, multi-walled CNC (MWCNC) grown by CCVD using an $Fe(CO)_5$-coated substrate and C_5H_5N feedstock gas [11,12] has been reported. Like the structure of CNTs, the structure of MWCNC is graphitic.

Figure 1 shows scanning electron microscopy (SEM) images of CNCs; CNC appears spring-like. The diameters of the coil fibers range from 100 to 200 nm, while the outer diameters of the coils range from 300 to 900 nm; the lengths of the coils are micrometer-scale [13–15]. The CNC fibers are composed of amorphous carbon and have structures similar to CMC.

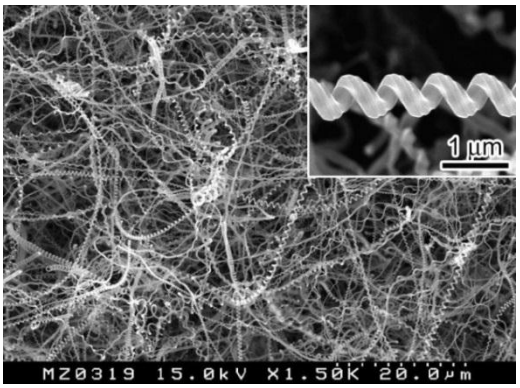

Figure 1. Scanning electron microscopy (SEM) micrograph of carbon nanocoils (CNCs).

The CCVD method is one of the most powerful techniques for synthesis of CNT, CNF, and CNC, although carbon nanomaterials can be synthesized using various methods including arc discharge and laser vaporization [15]. For the growth of CNCs, a combination of two types of catalysts, one with higher carbon segregation ability and another with lower carbon segregation ability, is employed [10,13,16,17]. The model of Motojima can be applied to explain the growth mechanism of CNCs [7]. Very recently, it was reported that a single type of metal catalyst can synthesize CNC by controlling its particle diameter [18]. Metal catalysts can be categorized not only by their carbon segregation abilities, but also by their synergetic effects with other catalysts on carbon segregation; these types of synergistic catalysts are called promoters. Table 1 shows the classification of catalysts.

Table 1. Classification of catalysts for carbon nanotubes (CNTs) and CNCs growth.

Role	Type of catalyst	Catalytic effect
Catalyst	Ni [7]	High ability of carbon segregation
	Fe [19]	
	Co [20], Pd [21]	
Promoter	Cu [10], Sn [19]	Low carbon segregation ability
	S [22]	Synergetic effect with catalyst
	In [23]	Keeps the distance between catalyst nanoparticles
	K [24]	Controls the coil diameter

Compared to CMCs, CNCs can be applied in electromagnetic absorption materials with shorter wavelengths [25]. They are also used in nanosprings [26–30], electrode materials in fuel cells [31–34], field emitters [35–37], magnetic sensors [38,39], and various industrial fields [40–42].

We have synthesized large quantities of CNCs by employing a drop-coating method that drops an Sn liquid solution mixed with Fe powder on a graphite substrate [43,44]. Using this method, the CNC purity on the surface of the deposits reached almost 100%. The CNCs formed a CNC layer with a micrometer-scale thickness. However, there was a carbon layer that did not contain CNCs between the upper and lower CNC layers; this was called the carbon layer. Both the CNC and carbon layers were grown from a catalyst that was deposited on the substrate. The catalyst is necessary to form solid carbon from gaseous feedstock in the CVD process. It was shown that the carbon layer exists like a "core" between the CNC layers [42]. When we took into account this carbon layer, the CNC purity over the whole deposits grown became 55%, very low compared to the purity of the CNC layer. The low CNC purity is ascribed to the thickness of the carbon layer. Yokota *et al*. [45] reported that the thickness of the carbon layer depends on the thickness of the catalyst film on the substrate.

In this study, we attempted to reduce the thickness of the catalyst layer by using a spin-coating method and Fe fine powder to increase the CNC yield and purity. We used an automatic CVD apparatus with an Fe_2O_3/SnO_2-coated substrate and C_2H_2/N_2 feedstock gas to synthesize the CNCs, and the produced CNCs were then observed by SEM.

2. Results and Discussion

2.1. Effect of Gas Flow Rate

We varied the flow rates of C_2H_2 feedstock and N_2 dilution gases between 100–400 mL/min and 1000–1800 mL/min, respectively. The catalyst structure on the substrate was $SnO_2/Fe_2O_3/SnO_2$, and the Fe/Sn molar ratio was 1:2.6. The spin-coating velocity was 1000 rpm, and the synthesis time was 10 min. The other CVD conditions were the same as those listed in Table 2. For the experiments where the N_2 gas flow rate was varied, the flow rate of C_2H_2 gas was fixed at 250 mL/min. When the C_2H_2 gas flow rate was varied, the flow rate of N_2 gas was fixed at 1400 mL/min.

The experimental results for the thicknesses of the CNC and carbon layers at fixed N_2 gas flow rate are shown in Figure 2; the *x*-axis is the flow rate ratio of N_2 to C_2H_2. A cross-sectional SEM micrograph of the CNC and carbon layers is shown in Figure 3a. When the flow rate of C_2H_2 gas was varied, the thicknesses of the CNC and carbon layers were maximized at a C_2H_2/N_2 gas flow ratio of 0.18 and

decreased for ratios >0.18. The difference in thickness between the CNC and carbon layers was also maximized at the ratio of 0.18. Similar results were obtained when the flow rate of N_2 gas was varied while that of C_2H_2 was kept constant. We carefully evaluated a number of SEM micrographs of the CNC layers and concluded that the CNC purity was ≥95% when the C_2H_2/N_2 gas flow ratio was within the green-colored range in Figures 2 and 3c. The C_2H_2/H_2 ratios outside of the green-colored range resulted in low CNC purities (Figure 3b).

Table 2. Catalytic vapor deposition (CCVD) conditions.

Catalyst precursor	**Fe_2O_3 fine powder (Diameter: 20 nm, Nilaco, Tokyo, Japan) SnO_2 drop-coating solution (0.13 M, Kojundo Chemical Laboratory, Sakado, Japan)**
Spin-coating velocity	1000–2500 rpm
Catalyst structure	Fe_2O_3/SnO_2, $SnO_2/Fe_2O_3/SnO_2$, SnO_2/Fe_2O_3
Catalyst molar ratio	Fe:Sn = 1:2.6–1:13
Feedstock gas (flow rate)	C_2H_2 (100–400 mL/min)
Dilution gas (flow rate)	N_2 (1000–1800 mL/min)
Synthesis temperature	780 ℃
Synthesis time	0.5–30 min
Annealing temperature	780 ℃
Annealing time	5 min

These results shown above indicate that when the C_2H_2/N_2 gas flow ratio was low, CNC growth was not effective due to the shortage of feedstock gas. On the other hand, when the C_2H_2/N_2 gas flow ratio was too high, excess C_2H_2 molecules were supplied to the catalyst nanoparticles, decreasing their catalytic activity. In this study, a C_2H_2/N_2 flow rate ratio of 0.18 gave the highest CNC yield and the lowest compositional ratio of the carbon layer to the CNC layer in the deposit [15].

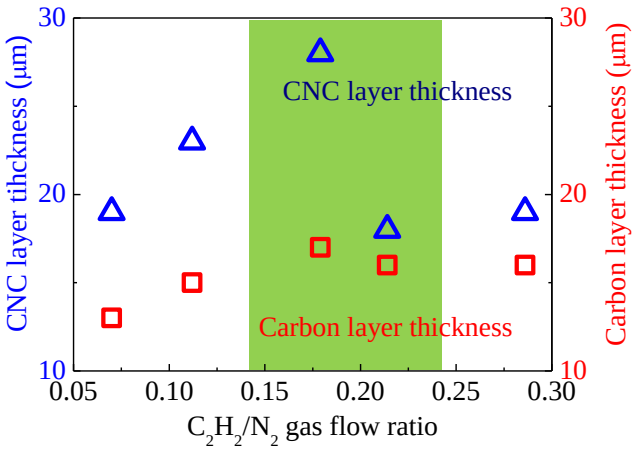

Figure 2. Thicknesses of CNC and carbon layers *vs.* C_2H_2/N_2 gas flow ratio. The flow rate of N_2 gas was fixed at 1400 mL/min, while that of C_2H_2 gas was varied. The green-colored area represents the range for which the CNC purity in the CNC layer was 95%–100%.

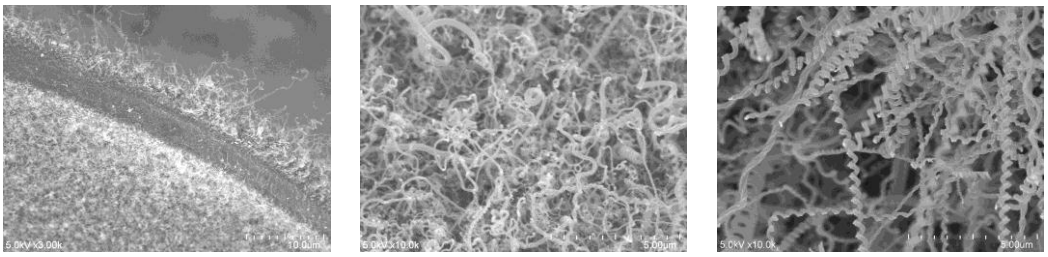

(**a**) (**b**) (**c**)

Figure 3. SEM micrographs of carbon deposits: (**a**) cross-sectional view of CNC and carbon layers; (**b**) the surface of a low-purity CNC layer; and (**c**) the surface of a high-purity CNC layer. In (**a**), the relatively dark area shows a carbon layer that does not contain CNCs; many CNCs were observed in the other area, which is called the CNC layer.

2.2. Effect of Spin-Coating Velocity and Synthesis Time

The effect of spin-coating velocity on catalyst film deposition on the substrate was examined by varying the spin-coating velocity between 1000 and 2500 rpm. The catalyst structure on the substrate was Fe_2O_3/SnO_2, and the Fe/Sn molar ratio was 1:2.6. The flow rates of C_2H_2 feedstock and N_2 dilution gases were 250 mL/min and 1400 mL/min, respectively, and the synthesis time was 10 min. The other CVD conditions are the same as those listed in Table 2.

Figure 4 shows the cross-sectional SEM micrographs of the deposits with spin-coating velocities of 1000 and 1500 rpm. The surfaces of CNC layers in Figure 4 are shown in Figure 5, and the correlations between the thicknesses of the CNC and carbon layers and the spin-coat velocity are shown in Figure 6.

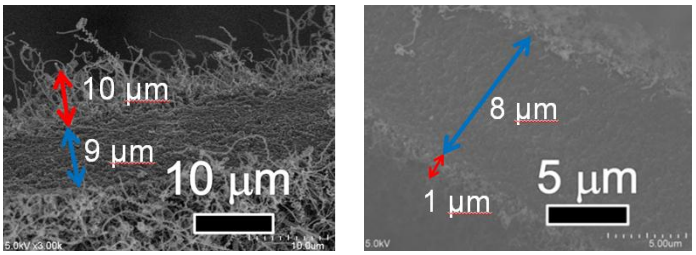

(**a**) (**b**)

Figure 4. Cross-sectional SEM micrographs of deposits including CNC and carbon layers obtained at spin-coating velocities of (**a**) 1000 and (**b**) 1500 rpm. The red and blue arrows represent the thicknesses of CNC and carbon layers, respectively.

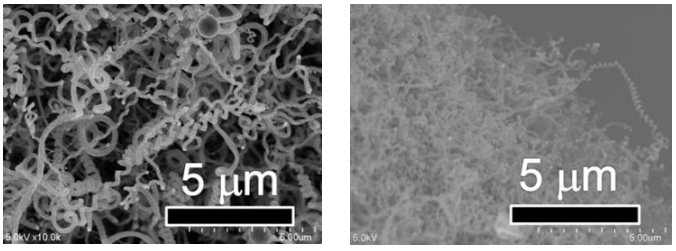

(**a**) (**b**)

Figure 5. SEM micrographs of CNC layers obtained at spin-coating velocities of (**a**) 1000 and (**b**) 1500 rpm.

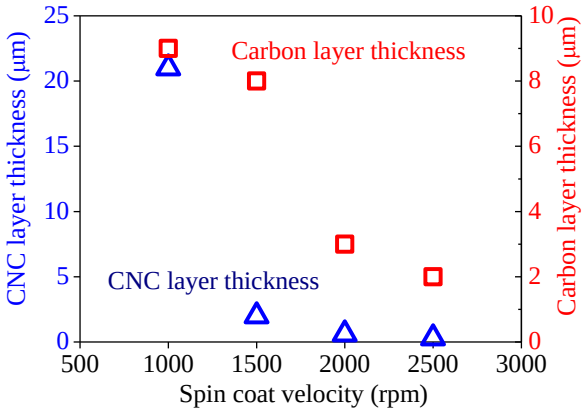

Figure 6. Thicknesses of CNC and carbon layers *vs.* spin-coat velocity. The synthesis time was 10 min.

The carbon layer thickness decreased with increasing spin-coating velocity because the catalyst film thinned with increasing spin-coating velocity. As the velocity was increased from 1000 to 2500 rpm, the film thickness was reduced because some of the liquid solution of Fe_2O_3 and SnO_2 was blown from the substrate, decreasing the amount of liquid coated on the substrate. When the spin-coating velocity was 1000 rpm, the CNC layer was formed; however, the CNC layer was hardly formed at a spin-coating velocity of 1500 rpm and higher. This might result from the inability to build up a stable basement for CNC growth. CNCs were reported to grow preferentially from a catalyst fixed on the dimples of a substrate surface [46]. In the described experiment, the carbon layer acted as a stable basement for CNC growth. If the thickness of the carbon layer became thin, CNC growth became more difficult. As a result, the optimal spin-coating velocity was 1000 rpm; this velocity resulted in the highest CNC purity, although the thickness of the carbon layer was also the highest at this velocity.

We then obtained the effect of the synthesis time by testing times between 30 s and 30 min (Figure 7).

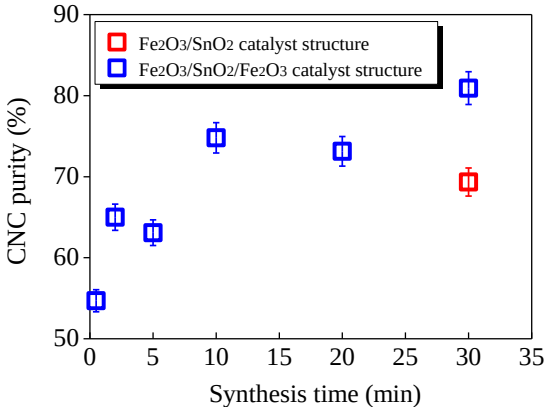

Figure 7. CNC purity *vs.* synthesis time at spin-coating velocity of 1000 rpm.

As synthesis time increased from 30 s to 10 min, the CNC purity increased constantly. However, the CNC purity remained almost constant at 75% for synthesis times between 10 min and 30 min, indicating saturation tendency.

2.3. Effect of Catalyst Structure

The influence of catalyst structure on carbon deposition was examined by testing catalyst structures of Fe_2O_3/SnO_2, $SnO_2/Fe_2O_3/SnO_2$, and SnO_2/Fe_2O_3 with a spin-coating velocity of 1000 rpm. The Fe/Sn molar ratio was 1:2.6, and the flow rates of C_2H_2 feedstock and N_2 dilution gases were 250 mL/min and 1400 mL/min, respectively. The synthesis time was 30 min. The other CVD conditions are the same as those listed in Table 2.

Figure 8 shows cross-sectional SEM micrographs of the carbon deposits including CNC and carbon layers grown from the three types of catalyst structures. The surfaces of the CNC layers are shown in Figure 9.

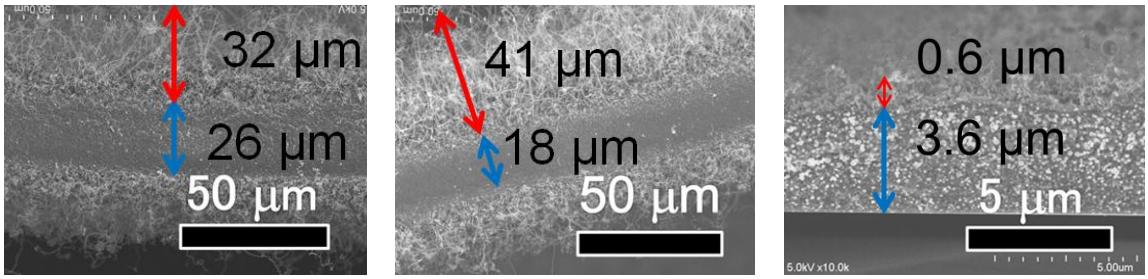

(**a**) (**b**) (**c**)

Figure 8. Cross-sectional SEM micrographs of carbon deposits grown with different catalyst structures: (**a**) Fe_2O_3/SnO_2; (**b**) $SnO_2/Fe_2O_3/SnO_2$; and (**c**) SnO_2/Fe_2O_3. The red and blue arrows represent the thicknesses of the CNC and carbon layers, respectively.

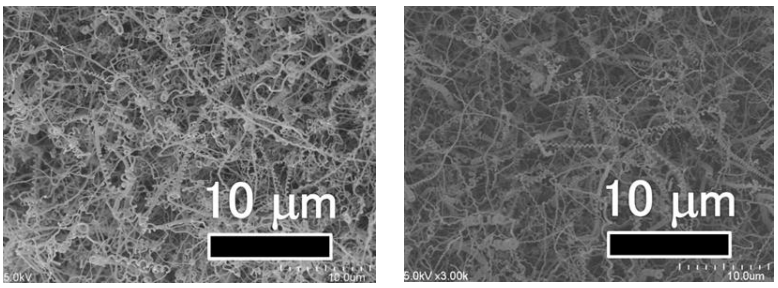

(**a**) (**b**)

Figure 9. SEM micrographs of the surfaces of CNC layers grown from different catalyst structures: (**a**) Fe_2O_3/SnO_2 and (**b**) $SnO_2/Fe_2O_3/SnO_2$. No CNCs were observed on the SnO_2/Fe_2O_3 catalyst structure.

As shown in Figure 8, CNC layers were formed on the (a) Fe_2O_3/SnO_2; and (b) $SnO_2/Fe_2O_3/SnO_2$ catalyst structures; the CNC purities on their surfaces ranged from 95% to 100%. The CNC purities were evaluated by Equation (1) to be 69% ± 2% and 81% ± 2% for the Fe_2O_3/SnO_2 and $SnO_2/Fe_2O_3/SnO_2$ catalyst structures, respectively. The difference in the CNC purity is attributed to the different growth models of the Fe_2O_3/SnO_2 and $SnO_2/Fe_2O_3/SnO_2$ catalyst structures (Figure 10).

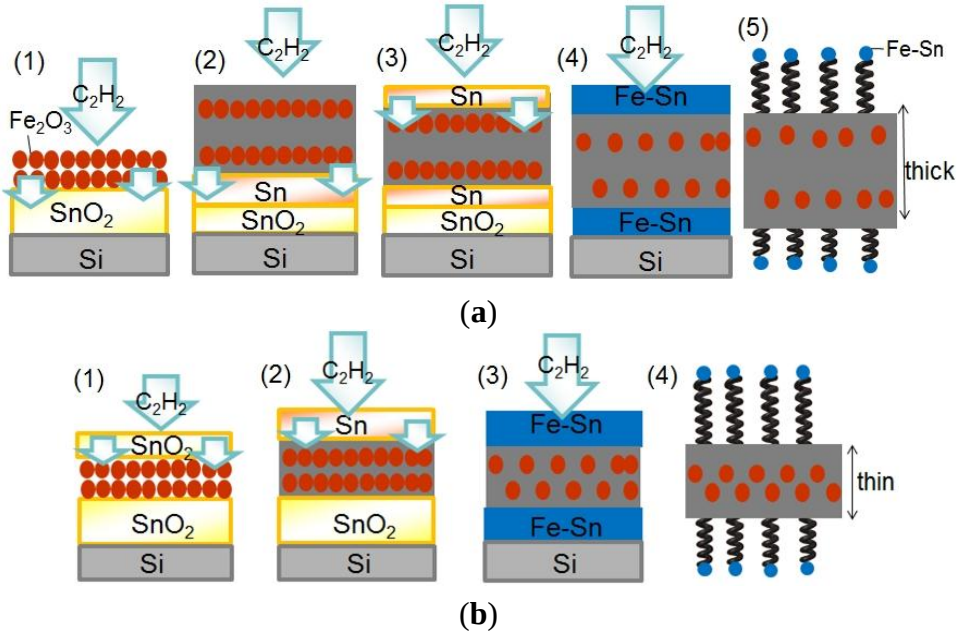

Figure 10. Growth models of (**a**) Fe_2O_3/SnO_2 and (**b**) $SnO_2/Fe_2O_3/SnO_2$ catalyst structures.

When C_2H_2 feedstock gas molecules are directly supplied to Fe_2O_3 on the Fe_2O_3/SnO_2 catalyst, the Fe_2O_3 forms nanoparticles that uptake carbon atoms inside them ((1) in Figure 10a). A portion of the C_2H_2 molecules pass through the Fe_2O_3 and reach SnO_2, which is partly reduced by the C_2H_2 molecules. The melting point of reduced Sn is 232 °C, which is much lower than that of SnO_2 (1127 °C). Therefore, the reduced Sn remains in the liquid phase at the CVD temperature. A portion of the Sn diffuses around the surface of the Fe_2O_3/SnO_2 structure ((2) in Figure 10a). This phenomenon is explained by a previous study in which the melted Sn diffuses through the fine pores in a Fe_2O_3 thin film by capillary action [44]. By supplying more C_2H_2 molecules Fe–Sn alloy forms on the surface of the Fe_2O_3/SnO_2 structure ((3) in Figure 10a), causing the formation of sheet-like carbon deposits on which CNCs are observed ((4) in Figure 10a). In the Fe_2O_3/SnO_2 catalyst structure, C_2H_2 molecules are directly supplied to Fe_2O_3, which has a strong carbon segregation ability, resulting in the formation of a quite thick carbon layer.

The growth model of the $SnO_2/Fe_2O_3/SnO_2$ catalyst structure is shown in Figure 10b. The amount of C_2H_2 molecules that reach the Fe_2O_3 catalyst nanoparticles is limited. This phenomenon is similar to that observed for the SnO_2/Fe_2O_3 catalyst structure, which resulted in almost no CNC growth (Figure 8b). However, in our experimental conditions, the molar quantity of the upper Sn in $SnO_2/Fe_2O_3/SnO_2$ was half that of the Sn in SnO_2/Fe_2O_3, resulting in the uptake of more carbon atoms inside the Fe_2O_3 catalyst nanoparticles of $SnO_2/Fe_2O_3/SnO_2$. By supplying more C_2H_2 molecules, Fe–Sn alloys form on the upper and lower surfaces of $SnO_2/Fe_2O_3/SnO_2$, similar to the case of Fe_2O_3/SnO_2 ((3) in Figure 10b). The CNCs are grown from the Fe–Sn alloys ((4) in Figure 10b). In $SnO_2/Fe_2O_3/SnO_2$, the amount of C_2H_2 molecules supplied to Fe_2O_3, which has a high carbon segregation ability, was less than in the case of Fe_2O_3/SnO_2. Therefore, the thickness of the carbon layer grown on $SnO_2/Fe_2O_3/SnO_2$ was thin. More C_2H_2 molecules were used to form the CNC layer instead of the carbon layer. This explains the experimental result shown in Figure 8, in which the thickness of the CNC layer grown from $SnO_2/Fe_2O_3/SnO_2$ was larger than that grown from Fe_2O_3/SnO_2.

In both of the above models, C_2H_2 diffusion in the catalyst thin film is an important process for the growth of the CNC layer. This implies a difference in thickness between the upper and lower CNC layers; the upper layer always became thicker than the lower one, which is located on the other side of the feedstock supply. CNCs were hardly grown on the SnO_2/Fe_2O_3 catalyst structure; short and irregularly-shaped carbon fibers were grown instead. This is explained by the limited amount of C_2H_2 supplied to Fe_2O_3 due to the thick SnO_2 layer. Since the carbon segregation ability of Fe is significantly higher that of Sn, carbon growth hardly occurred on SnO_2/Fe_2O_3. From the above experimental results, we conclude that the $SnO_2/Fe_2O_3/SnO_2$ catalyst structure was most suitable to grow CNC in high yield and purity.

3. Experimental Section

3.1. Evaluation Method

In this study, we evaluated the purity of CNCs over the entire deposit. As illustrated in Figure 11, the carbon deposit is sheet-like in shape, and CNCs were grown on both sides of the carbon layer.

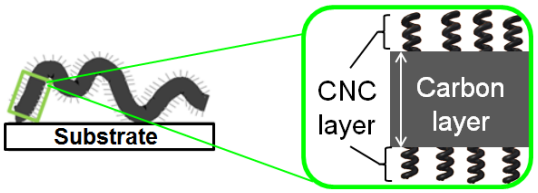

Figure 11. Illustration of the carbon deposit.

The CNC purity was defined by Equation (1):

$$\text{CNC purity} = \frac{\text{Thickness of CNC layer}}{\text{Thicknesses of CNC and carbon layers}} \times 100\ (\%) \quad (1)$$

We assumed the CNC purities in the CNC and the carbon layers to be 100% and 0%, respectively. This is consistent with the SEM observations of the deposits. The thickness of the CNC layer was obtained as the summation of the upper and lower layers. We examined the CVD conditions and catalyst formation methods in order to maximize the CNC yield and purity.

3.2. Catalyst Formation

We used a drop-coating method to deposit catalyst films on substrates, as reported in our previous study [44,45]. Although this method is convenient, the catalyst films tended to be thick under our experimental conditions. Thus, in this study, we instead employed a spin-coating method and also attempted to reduce the catalyst film thickness by replacing Fe powder (diameter: 1 and 3–5 μm) with a finer Fe power (diameter: 20 nm). Si was used as a substrate, and liquid solutions of Fe_2O_3 (0.1 M) and SnO_2 (0.13 M) were used as a catalyst precursor. The spin-coating velocity was varied between 1000 and 2500 rpm, and the Fe_2O_3 and SnO_2 liquids were spin-coated separately on the substrate. After one catalyst film was formed on the substrate, the substrate was dried at 80 ℃ for 5 min to avoid mixing the catalysts during the deposition of multi-layered catalyst thin films.

We investigated the most suitable catalyst structure for CNC growth and the reduction of carbon layer thickness by SEM observation of three types of catalyst structures: (a) Fe_2O_3/SnO_2; (b) SnO_2/Fe_2O_3; and (c) $SnO_2/Fe_2O_3/SnO_2$ (Figure 12).

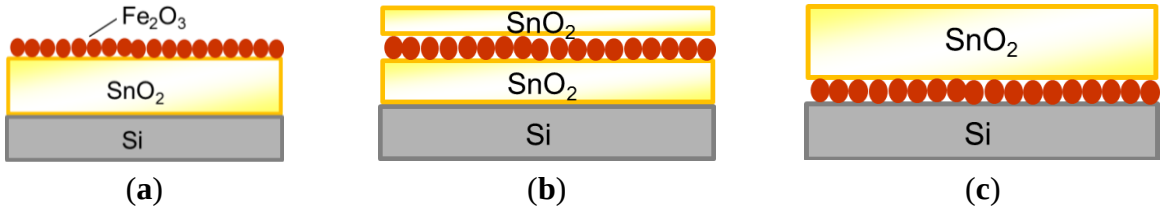

Figure 12. Catalyst structures formed in this study: (**a**) Fe_2O_3/SnO_2; (**b**) $SnO_2/Fe_2O_3/SnO_2$; and (**c**) SnO_2/Fe_2O_3 structures.

3.3. CVD Conditions

The CVD conditions in this study are listed in Table 2. Figure 13 shows a schematic illustration of the automatic CVD apparatus developed in our laboratory. The details of this apparatus are described elsewhere [47,48].

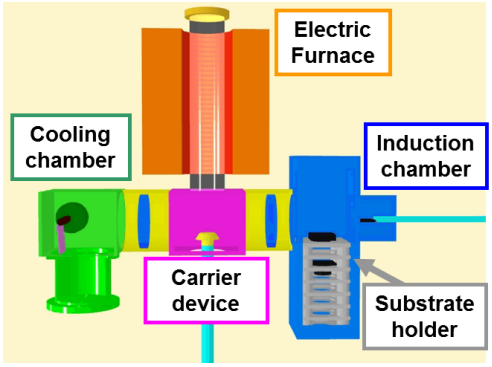

Figure 13. Schematic illustration of the automatic catalytic vapor deposition (CVD) apparatus.

4. Conclusions

CNCs have applications in field electron emitters, magnetic wave absorption materials, and nanosprings. However, CNC purity is still low in the carbon deposits as a whole, and improving the CNC purity is necessary for its industrial use. In this study, we attempted to reduce the compositional ratio of the carbon layer, which does not contain CNCs, to the CNC layer and performed CVD experiments.

We varied the flow rates of the feedstock and dilution gases and investigated the CVD conditions to obtain thick and high-purity CNC layers. In a previous study, we used a drop-coating method to deposit catalyst thin films; this resulted in a thick catalyst film and, as a consequence, a thick carbon layer. In this study, we used a spin-coating method to reduce the catalyst film thickness. We changed the diameter of the catalytic Fe powder using in catalyst film deposition from 1 or 3–5 μm to 20 nm to reduce the catalyst film thickness. In the optimization of CVD conditions, the spin-coating velocity and catalyst structure were varied. The identified optimal conditions allowed the formation of a thinner carbon layer and a thicker CNC layer, resulting in a high CNC purity. The CNC purity was improved from 55% (the highest in our previous studies) to 81% ±2% in this study.

Acknowledgments

This work was partly supported by the EIIRIS Project from Toyohashi University of Technology (TUT), JSPS KAKENHI Grant Numbers 24360108 and 25630110.

Author Contributions

Yoshiyuki Suda examined the experimental data and the mechanism of CNC growth in high yield and purity. Koji Maruyama and Tetsuo Iida performed CVD experiments, evaluated CNC growth, and proposed a CNC growth model. Hirofumi Takikawa, Hitoshi Ue, Kazuki Shimizu, and Yoshito Umeda discussed the experimental data.

Conflicts of Interest

The authors declare no conflict of interest.

References

1. Sugioka, Y.; Yokota, M.; Pude, T.; Suda, Y.; Takikawa, H.; Tanoue, H.; Ue, H.; Umeda, Y.; Shimizu, K. Effect of filament discharge on upright of carbon nanotwists tightly-adhered to substrate. *Jpn. J. Appl. Phys.* **2011**, *50*, doi:10.1143/JJAP.50.08JF08.
2. Kroto, H.W.; Health, J.R.; O'Brien, S.C.; Curl, R.F.; Smally, R.E. C_{60}: Buckminsterfulleren. *Nature* **1985**, *318*, 162–163.
3. Iijima, S. Helical microtubules of graphitic carbon. *Nature* **1991**, *354*, 56–58.
4. Ihara, S.; Itoh, S. Helically coiled and toroidal cage forms of graphitic carbon. *Carbon* **1995**, *33*, 931–939.
5. Nishimura, K.; Kim, Y.A.; Matsushita, T.; Hayashi, T.; Endo, M. Structural characterization of boron-doped submicron vapor-grown carbon fibers and their anode performance. *J. Mater. Res*. **2000**, *15*, 1303–1313.
6. Motojima, S.; Kawaguchi, M.; Nozaki, K.; Iwanaga, H. Growth of regularly coiled carbon filaments by Ni catalyzed pyrolysis of acetylene, and their morphology and extension characteristics. *Appl. Phys. Lett.* **1990**, *56*, 321–323.
7. Motojima, S.; Chen, Q. Three-dimensional growth mechanism of cosmo-mimetic carbon microcoils obtained by chemical vapor deposition. *J. Appl. Phys*. **1999**, *85*, 3919–3921.
8. Zhang, M.; Nakayama, Y.; Pan, L. Synthesis of carbon tubule nanocoils in high yield using iron-coated indium tin oxide as catalyst. *Jpn. J. Appl. Phys.* **2000**, *39*, 1242–1244.
9. Pan, L.; Hayashida, T.; Harada, A.; Nakayama, Y. Effects of iron and indium tin oxide on the growth of carbon tubule nanocoils. *Phys. B* **2002**, *323*, 350–351.
10. Katsumata, T.; Fujimura, Y.; Nagayama, M.; Tabata, H.; Takikawa, H.; Hibi, Y.; Sakakibara, T.; Itoh, S. Synthesis of twisted carbon nanofiber by catalytic CVD method. *Trans. Mater. Res. Soc. Jpn.* **2004**, *29*, 501–504.
11. Lu, M.; Liu, W.M.; Guo, X.Y.; Li, H.L. Coiled carbon nanotubes growth via reduced-pressure catalytic chemical vapor deposition. *Carbon* **2004**, *42*, 805–811.
12. Bajpai, V.; Dai, L.; Ohashi, T. Large-scale synthesis of perpendicularly aligned helical carbon nanotubes. *J. Am. Chem. Soc*. **2004**, *126*, 5070–5071.

13. Takikawa, H.; Yatsuki, M.; Miyano, R.; Nagayama, M.; Sakakibara, T.; Itoh, S.; Ando, Y. Amorphous carbon fibrilliform nanomaterials prepared by chemical vapor deposition. *Jpn. J. Appl. Phys.* **2000**, *39*, 5177–5179.
14. Mcllroy, D.N.; Zhang, D.; Kranov, Y.; Norton, M.G. Nanosprings. *Appl. Phys. Lett.* **2001**, *79*, 1540–1542.
15. Suda, Y.; Takikawa, H.; Tanoue, H. Syntheses and Electronic Applications of Helical Carbon Nanofibers. In *Carbon Nanotubes*/*Book 2*; INTECH: Rijeka, Croatia, 2011; pp. 37–70.
16. Yang, S.; Chen, X.; Kikuchi, N.; Motojima, S. Catalytic effects of various metal carbides and Ti compounds for the growth of carbon nanocoils. *Mater. Sci.* **2008**, *62*, 1462–1465.
17. Yokota, M.; Suda, Y.; Takikawa, H.; Ue, H.; Shimizu, K.; Umeda, Y. Structural analysis of multi-walled carbon nanocoils synthesized with Fe–Sn catalyst supported on zeolite. *J. Nanosci. Nanotechnol.* **2011**, *11*, 2344–2348.
18. Wang, G.; Ran, G.; Wan, G.; Yang, P.; Gao, Z.; Lin, S.; Fu, C.; Qin, Y. Size-Selective Catalytic Growth of Nearly 100% Pure Carbon Nanocoils with Copper Nanoparticles Produced by Atomic Layer Deposition. *ACS Nano* **2014**, *8*, 5330–5338.
19. Hirahara, K.; Nakayama, Y. The effect of a tin oxide buffer layer for the high yield synthesis of carbon nanocoils. *Carbon* **2013**, *56*, 264–270.
20. Sun, L.F.; Mao, J.M.; Pan, Z.W.; Chang, B.H.; Zhou, W.Y.; Wang, G.; Qian, L.X.; Xie, S.S. Growth of straight nanotubes with a cobalt-nickel catalyst by chemical vapor deposition. *Appl. Phys. Lett.* **1999**, *74*, 644–646.
21. Nitze, F.; Abou-Hamad, E.; Wagberg, T. Carbon nanotubes and helical carbon nanofibers grown by chemical vapour deposition on C60 fullerene supported Pd nanoparticles. *Carbon* **2011**, *49*, 1101–1107.
22. Wei, J.; Zhu, H.; Jia, Y.; Shu, Q.; Li, C.; Wang, K.; Wei, B.; Zhu, Y.; Wang, Z.; Luo, J.; *et al.* The effect of sulfur on the number of layers in a carbon nanotube. *Carbon* **2007**, *45*, 2152–2158.
23. Wang, W.; Yang, K.; Gaillard, J.; Bandaru, P.R.; Rao, A.M. Rational synthesis of helically coiled carbon nanowires and nanotubes through the use of tin and indium catalysts. *Adv. Mater.* **2008**, *20*, 179–182.
24. Tsou, T.Y.; Lee, C.Y.; Chiu, H.T. K and Au bicatalyst assisted growth of carbon nanocoils from acetylene: effect of deposition parameters on field emission properties. *ACS Appl. Mater. Interfaces* **2012**, *4*, 6505–6511.
25. Eguchi, U.; Takikawa, H.; Suda, Y. Electromagnetic wave absorption characteristics of multi-walled carbon nano-coils. *Jpn. J. Appl. Phys.* **2014**, *53*, doi:10.7567/JJAP.53.045102.
26. Wiliiams, K.L.; Köhler, J.; Boman, M. Fabrication and mechanical characterization of LCVD-deposited carbon micro-springs. *Sens. Actuators A* **2006**, *130–131*, 358–364.
27. Feng, C.; Liew, K.M. Structural stability of carbon nanosprings. *Carbon* **2011**, *49*, 4688–4694.
28. Yonemura, T.; Suda, Y.; Tanoue, H.; Takikawa, H.; Ue, H.; Shimizu, K.; Umeda, Y. Torsion fracture of carbon nanocoils. *J. Appl. Phys.* **2012**, *112*, doi:10.1063/1.4758921.
29. Lim, S.L.; Suda, Y.; Takimoto, K.; Ishii, Y.; Tanoue, H.; Takikawa, H.; Ue, H.; Shimizu, K.; Umeda, Y. Optimization of chemical vapor deposition for reducing the fiber diameter and number of graphene layers in multi-walled carbon nanocoils. *Jpn. J. Appl. Phys.* **2013**, *52*, doi:10.7567/JJAP.52.11NL04.
30. Yonemura, T.; Suda, Y.; Shima, H.; Tanoue, H.; Takikawa, H.; Ue, H.; Shimizu, K.; Umeda, Y. Real-time deformation of carbon nanocoils under axial loading. *Carbon* **2015**, *83*, 183–187.

31. Sevilla, M.; Sanchis, C.; Valdes-Solis, T.; Morallon, E.; Fuertes, A.B. Highly dispersed platinum nanoparticles on carbon nanocoils and their electrocatalytic performance for fuel cell reactions. *Electrochim. Acta* **2009**, *54*, 2234–2238.
32. Lim, S.L.; Takimoto, K.; Ishii, Y.; Suda, Y.; Tanoue, H.; Takikawa, H.; Ue, H.; Shimizu, K.; Umeda, Y. Improvement of growth yield of multi-walled carbon nanocoils by mesoporous materials and Sn amount. *Trans. MRS Jpn.* **2011**, *36*, 469–473.
33. Suda, Y.; Ozaki, M.; Tanoue, H.; Takikawa, H.; Ue, H.; Shimizu, K.; Muramoto, H. Supporting PtRu catalysts on various types of carbon nanomaterials for fuel cell applications. *J. Phys.* **2013**, *433*, doi:10.1088/1742-6596/433/1/012008.
34. Suda, Y.; Kaida, S.; Ozaki, M.; Shimizu, Y.; Okabe, Y.; Tanoue, H.; Takikawa, H.; Ue, H.; Shimizu, K. Use of carbon nanocoil as a catalyst support in direct methanol fuel cell. *AIP Conf. Proc.* **2014**, *1585*, 77–88.
35. Pan, L.; Konishi, Y.; Tanaka, H.; Sueoka, O.; Nosaka, T.; Nakayama, Y. Effect of morphology on field emission properties of carbon nanocoils and carbon nanotubes. *Jpn. J. Appl. Phys.* **2005**, *44*, 1652–1654.
36. Hokushin, S.; Pan, L.; Konishi, Y.; Tanaka, H.; Nakayama, Y. Field emission properties and structural changes of a stand-alone carbon nanocoil. *Jpn. J. Appl. Phys.* **2007**, *46*, 565–567.
37. Hosokawa, Y.; Shinohara, Y.; Yokota, M.; Shiki, H.; Suda, Y.; Oke, S.; Takikawa, H.; Ina, T.; Morioki, M.; Fujimura, Y.; *et al*. Filament discharge enhances field emission properties by making twisted carbon nanofibres stand up. *J. Phys. D* **2008**, *41*, doi:10.1088/0022-3727/41/20/205418.
38. Fujii, M.; Matsui, M.; Motojima, S.; Hishikawa, Y. Magnetoresistance in carbon micro-coils annealed at various temperatures. *J. Cryst. Growth* **2002**, *237–239*, 1937–1941.
39. Yamamoto, K.; Hirayama, T.; Kusunoki, M.; Yang, S.; Motojima, S. Electron holographic observation of micro-magnetic fields current-generated from single carbon coil. *Ultramicroscopy* **2006**, *106*, 314–319.
40. Katsuno, T.; Chen, X.; Yang, S.; Motojima, S.; Homma, M.; Maeno, T.; Konyo, M. Observation and analysis of percolation behavior in carbon microcoils/silicone-rubber composite sheets. *Appl. Phys. Lett.* **2006**, *88*, doi:10.1063/1.2206701.
41. Fujiyama, Y.; Tomokane, R.; Tanaka, K.; Akita, S.; Higashi, Y.; Pan, L.; Nosaka, T.; Nakayama, Y. Alignment of carbon nanocoils in polymer matrix using dielectrophoresis. *Jpn. J. Appl. Phys.* **2008**, *47*, 1991–1993.
42. Maruyama, K.; Suda, Y.; Tanoue, H.; Takikawa, H.; Ue, H.; Shimizu, K.; Umeda, Y. Improved mechanical properties of bucky paper achieved via the addition of carbon nanocoils. *AIP Conf. Proc.* **2014**, *1585*, 89–96.
43. Xu, G.; Chen, B.; Shiki, H.; Katsumata, T.; Takikawa, H.; Sakakibara, T.; Itoh, S.; Ina, T. Parametric study on growth of carbon nanocoil by catalytic chemical vapor deposition. *Jpn. J. Appl. Phys.* **2005**, *44*, 1569–1576.
44. Suda, Y.; Ishii, Y.; Miki, T.; Maruyama, K.; Tanoue, H.; Takikawa, H.; Ue, H.; Shimizu, K.; Umeda, Y. Improvement of carbon nanocoil purity achieved by supplying catalyst molecules from the vapor phase in chemical vapor deposition. *J. Mater. Res.* **2014**, *29*, 2179–2187.

45. Yokota, M.; Shinohara, Y.; Kawabata, T.; Takimoto, K.; Suda, Y.; Oke, S.; Takikawa, H.; Fujimura, Y.; Yamaura, T.; Itoh, S.; *et al*. Splitting and flattening of helical carbon nanofibers by acid treatment. *J. Nanosci. Nanotechnol.* **2010**, *10*, 3910–3914.
46. Li, D.; Pan, L. Necessity of base fixation for helical growth of carbon nanocoils. *J. Mater. Res.* **2012**, *27*, 431–439.
47. Hosokawa, Y.; Shiki, H.; Shinohara, Y.; Yokota, M.; Takikawa, H.; Ina, T.; Okada, F.; Fujimura, Y.; Yamaura, T.; Itoh, S.; *et al*. Preparation of powdery carbon nanotwist and application to printed field emitter. *Res. Lett. Mater. Sci.* **2007**, *2007*, doi:10.1155/2007/59167.
48. Sugioka, Y.; Suda, Y.; Tanoue, H.; Takikawa, H.; Ue, H.; Shimizu, K.; Umeda, Y. Effects of dielectric barrier discharge treatment conditions on the uprightness of carbon nanofibers. *IEEE Trans. Plasma Sci.* **2012**, *40*, 1794–1800.